Geophysical Journal International

Geophys. J. Int. (2013) **192,** 986–999 doi: 10.1093/gji/ggs100

Palaeointensity determinations and rock magnetic properties on basalts from Shatsky Rise: new evidence for a Mesozoic dipole low

C. Carvallo,[1] P. Camps,[2] M. Ooga,[3] G. Fanjat[2] and W. W. Sager[4]

[1] *Institut de Minéralogie et de Physique des Milieux Condensée, Université Pierre et Marie Curie, Paris, France. E-mail: carvallo@impmc.upmc.fr*
[2] *Géosciences Montpellier, CNRS and Université Montpellier* 2, *Montpellier, France*
[3] *Doshisha University, Kyoto, Japan*
[4] *Department of Oceanography, Texas A&M University, College Station,* TX 77843, *USA*

Accepted 2012 December 4. Received 2012 October 29; in original form 2012 February 6

SUMMARY

IODP Expedition 324 cored igneous rocks from Shatsky Rise, an oceanic plateau in the northwest Pacific Ocean that formed mainly during late Jurassic and Early Cretaceous times. We selected 60 samples from 3 different holes for Thellier–Thellier palaeointensity determinations. Induced and remanent magnetization curves measured at low- and high-temperature suggest a diverse and complex magnetic mineralogy, with large variations in Ti content and oxidation state. Hysteresis and FORC measurements show that most samples contain single-domain magnetic grains. After carrying out the palaeointensity determinations, only 9 samples satisfied all reliability criteria. These gave palaeointensity values between 16.5 and 21.5 μT, which correspond to average VDM values of $(4.9 \pm 0.2) \times 10^{22}$ Am^2 for an estimated age of 140–142 Ma. This value is lower than that for the recent field, which agrees with the hypothesis of a Mesozoic Dipole Low.

Key words: Palaeointensity; Rock and mineral magnetism; Ocean drilling.

1 INTRODUCTION

A strong knowledge of the long-term variations of palaeofield intensity is essential for a complete description of the geomagnetic field and its behaviour. Absolute palaeointensity data are difficult to recover because of the high failure rate of the widely used Thellier–Thellier method (Thellier & Thellier 1959). This method is the most reliable palaeointensity method because it reproduces the process of thermoremanent magnetization (TRM) acquisition by heating a sample in a laboratory field. As a result of the difficulty to obtain reliable results, the palaeointensity database is unevenly distributed throughout the geological time: seventy percent of palaeointensity data are concentrated in the last 20 Myr, whereas 35 per cent of the data span the last 1 Myr. We, therefore, lack a complete description of the geomagnetic field over many timescales, particularly beyond the last million years.

In particular, the experimental data published so far and gathered in the PINT database (Biggin *et al.* 2010) show that there is an ongoing controversy about the intensity of the geomagnetic field during the Mesozoic (250–65 Ma). By compiling data since Triassic time, Prévot *et al.* (1990) suggested the existence of a period of low field intensity between 100 and 200 Ma. This seemed to be confirmed by other studies: Perrin *et al.* (1991) from Jurassic continental tholeiites; Perrin & Shcherbakov (1997) by showing that the dipole nature of the field was preserved during the Mesozoic Dipole Low; Kosterov *et al.* (1998) in 133 Myr basalts from Brazil; and Shcherbakova *et al.* (2009) by revisiting palaeointensity results from baked contacts formed around 150 Ma in Armenia. Another study on lava flows in China formed just before the Cretaceous Normal Superchron (124–133 Ma; Zhu *et al.* 2003) and data from submarine basaltic glass also give virtual dipole moment (VDM) values that are lower than the present day VDM. In all these studies, most values are lower than 5×10^{22} Am^2. On the other hand, several recent studies mostly from lava flow from South America (Goguitchaichvili *et al.* 2002, 2008; Ruiz *et al.* 2006) did not show evidence for low values in this time range. A recent study on rocks from Mongolia also shows evidence for scattered, but mostly high VDM values (Shcherbakova *et al.* 2011). Data from submarine basaltic glass also give VDM values that are lower than the present day VDM (Tauxe 2006). However, considering that the average VDM on the interval 1–160 Myr is lower than the present day values, these authors suggest that the Mesozoic values are not abnormally low, but they are rather close to the average VDM, and concluded that the present day VDM is abnormally high instead. Obtaining new reliable experimental values for this time range is therefore important to resolve this discrepancy.

Ocean drilling has recovered basaltic rocks from Shatsky Rise (Fig. 1) at five sites. At Site 1213 on Tamu Massif (Fig. 2), Ocean Drilling Program (ODP) Leg 198 cored a 46-m section of basalt flows from beneath earliest Berriasian sediments (Shipboard

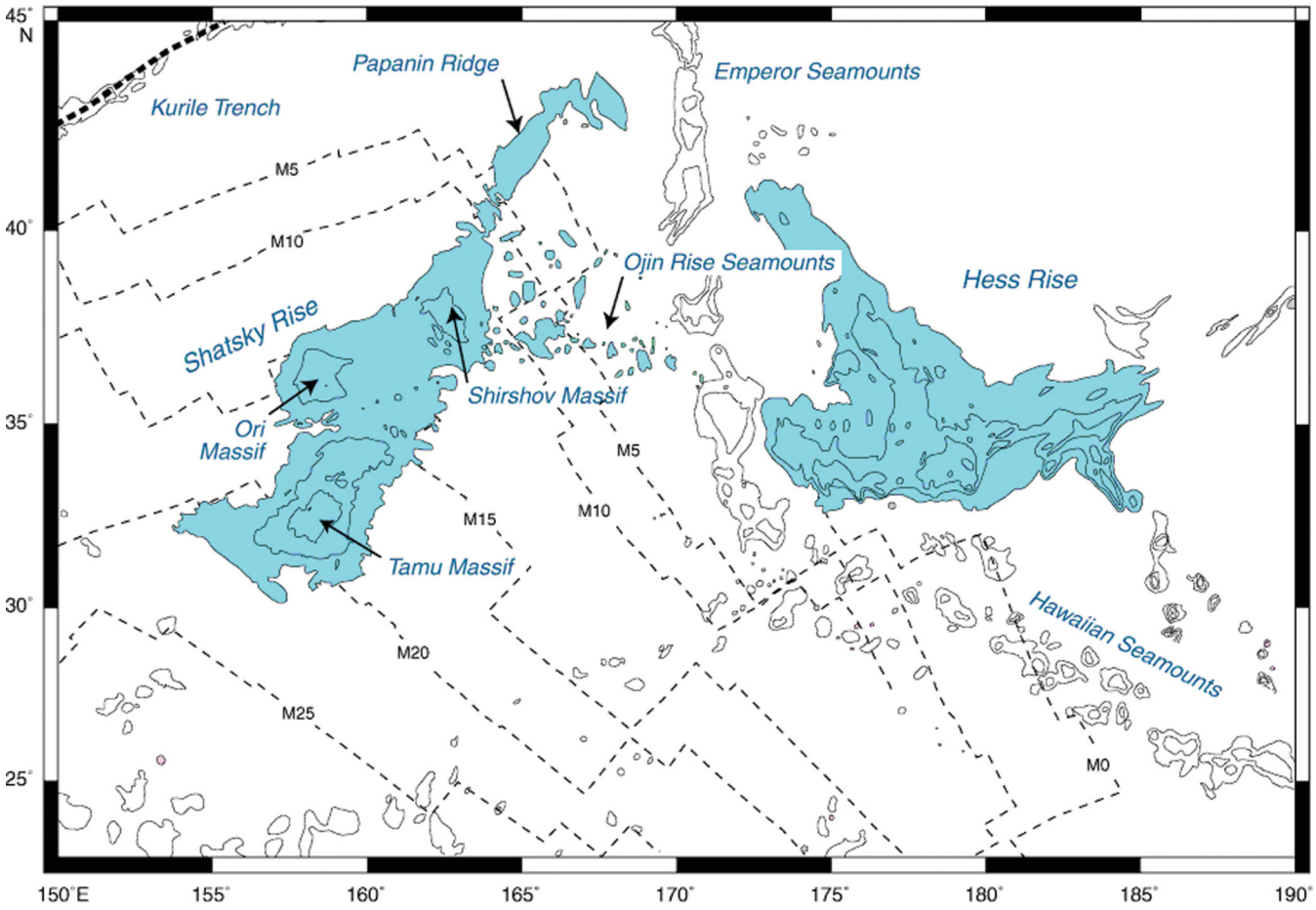

Figure 1. Location of Shatsky Rise, Hess Rise and selected magnetic anomaly lineations in the northwest Pacific Ocean. From Sager *et al.* (2010).

Scientific Party 2002). Palaeomagnetic analysis of Site 1213 basalt samples gives inclination values that are thought to be consistent with a reversed magnetic polarity (Tominaga *et al.* 2005). The mean $^{40}Ar/^{39}Ar$ age of two basalt samples from these flows is 144.6 ± 0.8 Ma (2σ; Mahoney *et al.* 2005), a value indistinguishable from the age of the Jurassic/Cretaceous boundary (145.5 Ma) and which correlates with magnetic Anomaly M18 or M19 in the Ogg & Smith (2004) timescale. Integrated Ocean Drilling Program (IODP) Expedition 324 recovered basalt flows at four more sites, U1347 on Tamu Massif, U1349 and U1350 on Ori Massif and U1346 on Shirshov Massif (Fig. 2; Sager *et al.* 2010). Coring at these sites penetrated 160m, 85 m, 173 m and 53 m of basaltic rocks, respectively. Rocks from sites U1347 and U1350 suffered only minor to moderate submarine alteration whereas those from sites U1346 and U1349 are moderately to severely altered (Sager *et al.* 2010). Although the ages of these rocks have not yet been determined, it is thought that Tamu Massif formed rapidly (Sager & Han 1993) and that other Shatsky Rise Massifs have ages near that of the underlying lithosphere, which is dated by magnetic lineations (Nakanishi *et al.* 1999). Thus, igneous rocks from sites U1349 and U1350 should be approximately 142–140 Ma because Ori Massif is bounded by magnetic anomalies M17-M16, whereas Site U1346 igneous rocks are approximately 136 Ma because Shirshov Massif is surrounded by anomalies M15-M14. The recovery of so many basalt samples from this period of the Mesozoic provides an opportunity to perform palaeointensity measurements on rocks of a period for which such measurements are few.

2 SAMPLING AND SHIPBOARD MEASUREMENTS

Routine palaeomagnetic measurements (thermal and alternating-field demagnetizations) were carried out on the Expedition 324 samples by the shipboard scientists (Sager *et al.* 2010). Although palaeoinclinations are negative and shallow for the basalt samples from Hole U1346A, those for Hole U1347A are mostly positive and shallow. The average inclination in Hole U1349A is close to zero. Finally, inclinations for the basalt samples from Hole U1350A are shallow, both positive and negative. Large scatter in palaeoinclination measurements were found in some units, similar to the results from Site 1213 (Tominaga *et al.* 2005), perhaps owing to large magnetic grain sizes that result in unstable primary magnetizations. Nevertheless, palaeoinclination averages within different flow units at each site are similar and imply that the time period covered by each igneous section is short (Sager *et al.* 2010).

We selected 60 samples for palaeointensity measurements from Holes U1347A, U1349A and U1350A. Because of the limited means of magnetic characterization on-board, we chose the samples based on their AF demagnetization spectra and variation of bulk susceptibility after each thermal demagnetization step: the demagnetization spectra must have an initial plateau which is characteristic of single-domain (SD) grains and the susceptibility variation during thermal demagnetization must be small, which gives an indication of thermal stability with heating. This behaviour was not observed in any of the Hole U1346A samples studied on-board, so no sample

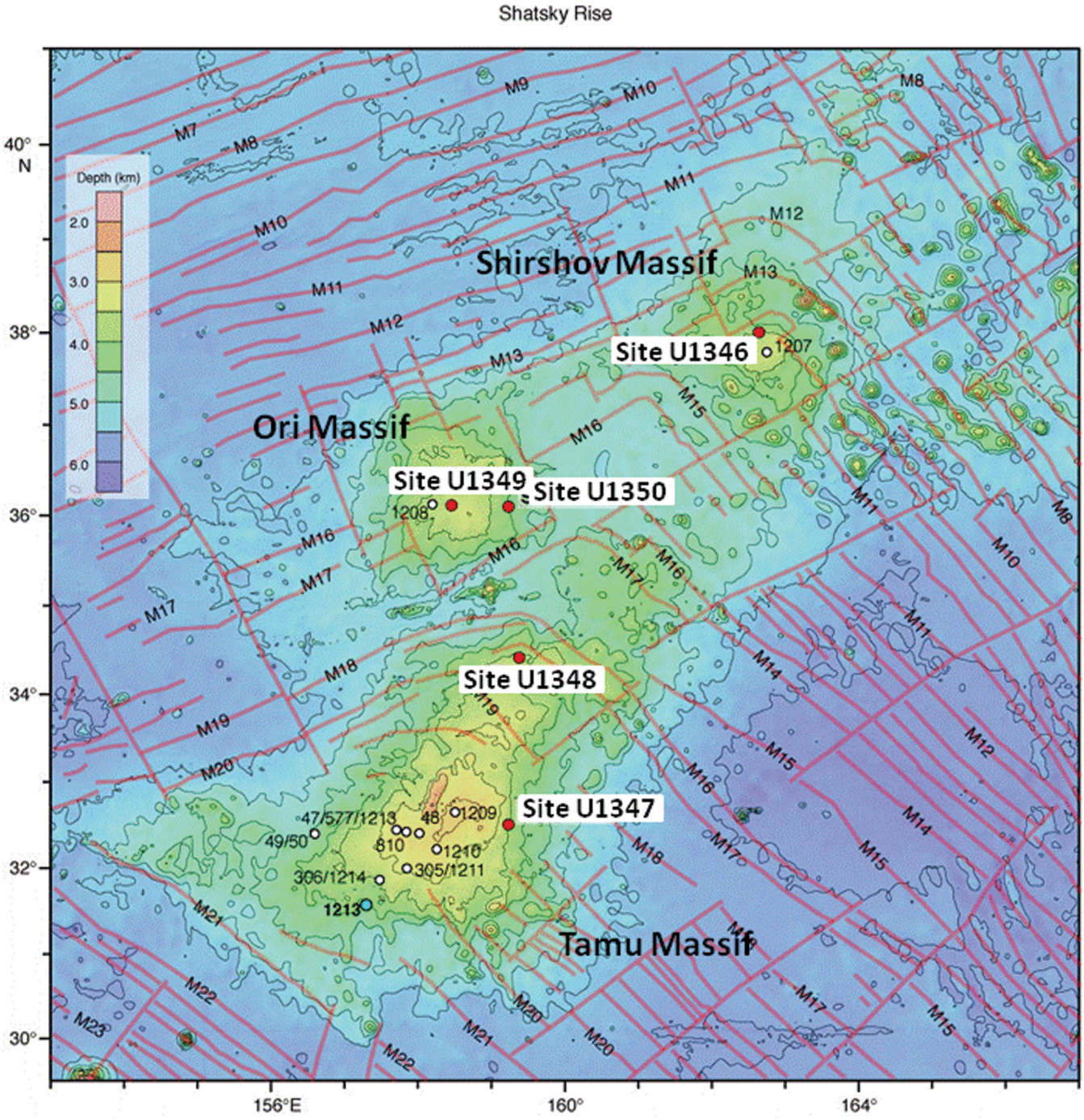

Figure 2. Magnetic lineations within and around Shatsky Rise and Expedition 324 sites (closed red circles). Heavy lines = magnetic lineations and fracture zones, open circles = prior drill sites, closed blue circle = location of Site 1213. Satellite-predicted bathymetry (Smith & Sandwell 1997) contours shown at 500 m intervals. Modified from Nakanishi *et al.* (1999) and Sager *et al.* (2010).

from this hole was selected for this study. We obtained 14 samples from Hole U1347A, all from the same massive basaltic flow (Unit XV in Sager *et al.* 2010); 22 samples from Hole U1349A, from five different subunits of the same lithological unit; and 24 samples from Hole U1350A: two from Unit IIc (stack of thin inflation units) and 22 from Unit IV (stack of ~0.1–0.5 m thick plagioclase-phyric pillow lavas). We tried to take two or three samples per pillow lava units or thin inflation units whenever it was possible.

Cylindrical specimens 2.5 cm in diameter were cut and trimmed to minicores 2-cm in length. The remaining material (usually a 1 or 2 mm slice) was kept for rock magnetic experiments. The minicores were oriented relative to the vertical axis of the core.

3 MAGNETIC PROPERTIES

All the magnetic properties measurements are shown in the IODP Data Report (Carvallo and Camps, in press). Here we show only representative examples with interpretations useful for palaeointensity determinations.

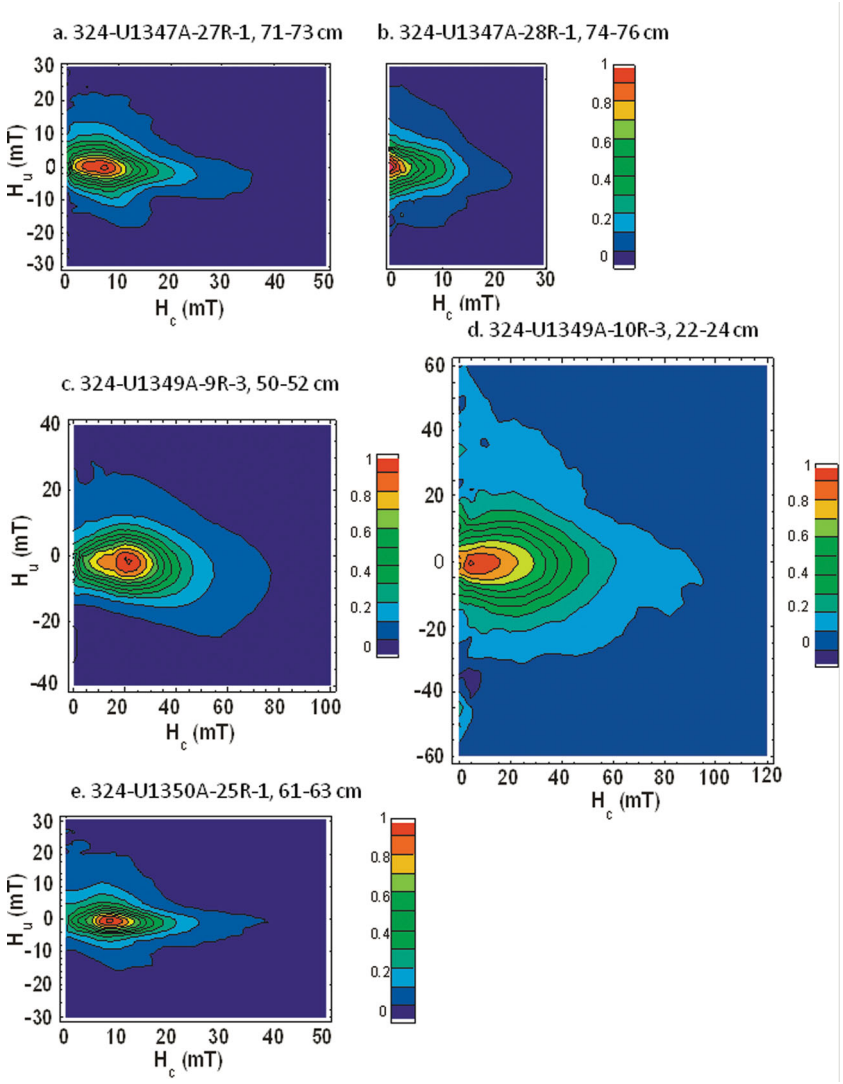

Figure 3. FORC diagrams of representative samples. Smoothing factors are set to 3 for all the diagrams. The vertical scale (H_u axis) is similar for the 5 diagrams, but not the horizontal scale (H_c axis).

3.1 FORC diagrams

First-Order Reversal Curve (FORC) diagrams allow a qualitative characterization of the magnetic domain structure and magnetostatic interactions even for materials containing a mixed grain size assemblage (Pike *et al.* 1999; Roberts *et al.* 2000). FORC diagrams were measured at the Laboratoire des Sciences du Climat et de l'Environnement (LSCE), Gif-sur-Yvette using an Alternating Gradient Magnetometer. One hundred FORCs were measured with an averaging time of 0.1 s. At least one sample per lava flow or unit was measured.

Hole U1347A: Coercive field values are fairly small for all the measured samples (lower than 8 mT except for one sample). However, most FORC diagrams are typical of single-domain grains, which are characterized by asymmetrical closed-contours around the peak of the distribution (Fig. 3a). FORC contours show some spreading around the $H_i = 0$ axis, with Full Width at Half-maximum (FWHM) between 5 and 15 mT, indicative of the presence of moderate interactions. One sample is more PSD-like, with contours that intersect the H_u axis (Fig. 3b).

Hole U1349A: Four of the five samples measured have relatively high coercive fields (between 14 and 25 mT). The FWHM values are between 12 and 34 mT, which is larger than the values for Holes U1347A and U1350A. All the FORC diagrams are SD-like (Fig. 3c for example) or PSD-like (Fig. 3d), as indicated by the closed-contours. Even though the FORC distribution peak occurs at fairly low coercivity, no MD behaviour (i.e. nearly vertical contours) could be detected in these samples.

Hole U1350A: The 17 FORC diagrams measured are all very similar. They display closed contours that are characteristic of SD particles, and the same amount of vertical spreading as the samples from Hole U1347A (Fig. 3e). FWHM values are all lower than 10 mT, indicating little interactions between magnetic grains.

According to these FORC diagrams, no MD behaviour could be detected in any of the 60 samples, but magnetostatic interactions seem to be present in samples from Holes U1347A and U1349A. This could violate Thellier's laws of additivity and reciprocity because pTRMs with non-overlapping blocking temperature ranges will have magnetostatic interactions. These pTRMs will, therefore, not be independent or additive. This could be a cause of failure

for Thellier–Thellier experiments (Levi 1977; Dunlop *et al.* 2005), though the claim has never been rigorously quantified. However, the FWHM of a profile of the distribution through the coercivity peak parallel to the H_i axis, which is usually used to quantify the amount of interactions, is smaller than 29 mT, the value suggested by Carvallo *et al.* (2006) as a threshold for pre-selection of samples for palaeointensity measurements using FORC diagrams. Therefore, no sample was rejected based on FORC diagrams.

3.2 Low temperature measurements

Low-temperature magnetization curves were measured with a Magnetic Properties Measurement System from Quantum Design at the Institut de Physique du Globe de Paris. A 2.5 T magnetic field was first applied in order for the samples to acquire a Saturation Isothermal Remanent Magnetization (SIRM), then the samples were cooled down to 10 K in zero-field, and their magnetization was measured during the cooling run. Subsequently, the samples were given another SIRM in a 2.5 T field at 10 K, and the samples were warmed up in zero-field to 300 K. The magnetization was measured during the heating run for at least one sample per lava flow.

Five different behaviours can be distinguished. The first behaviour is observed in 2 flows from Hole U1347A. A typical example is Sample 324-U1347A-26R-2, 89–91 cm (Fig. 4a). The room-temperature SIRM stays constant until cooling at 150 K and then decreases through a broad transition to 60 per cent of its original value. The low temperature SIRM increases with heating up to 120 K then decreases almost linearly to room temperature, reaching half its original value. This behaviour could indicate the presence of a very broad Verwey transition indicative of low-Ti content titanomagnetite.

The rest of the samples from Hole U1347A are characterized by a different behaviour (for example Sample 324-U1347A-28R-1, 74–76 cm, Fig. 4b): whereas the room-temperature SIRM varies very

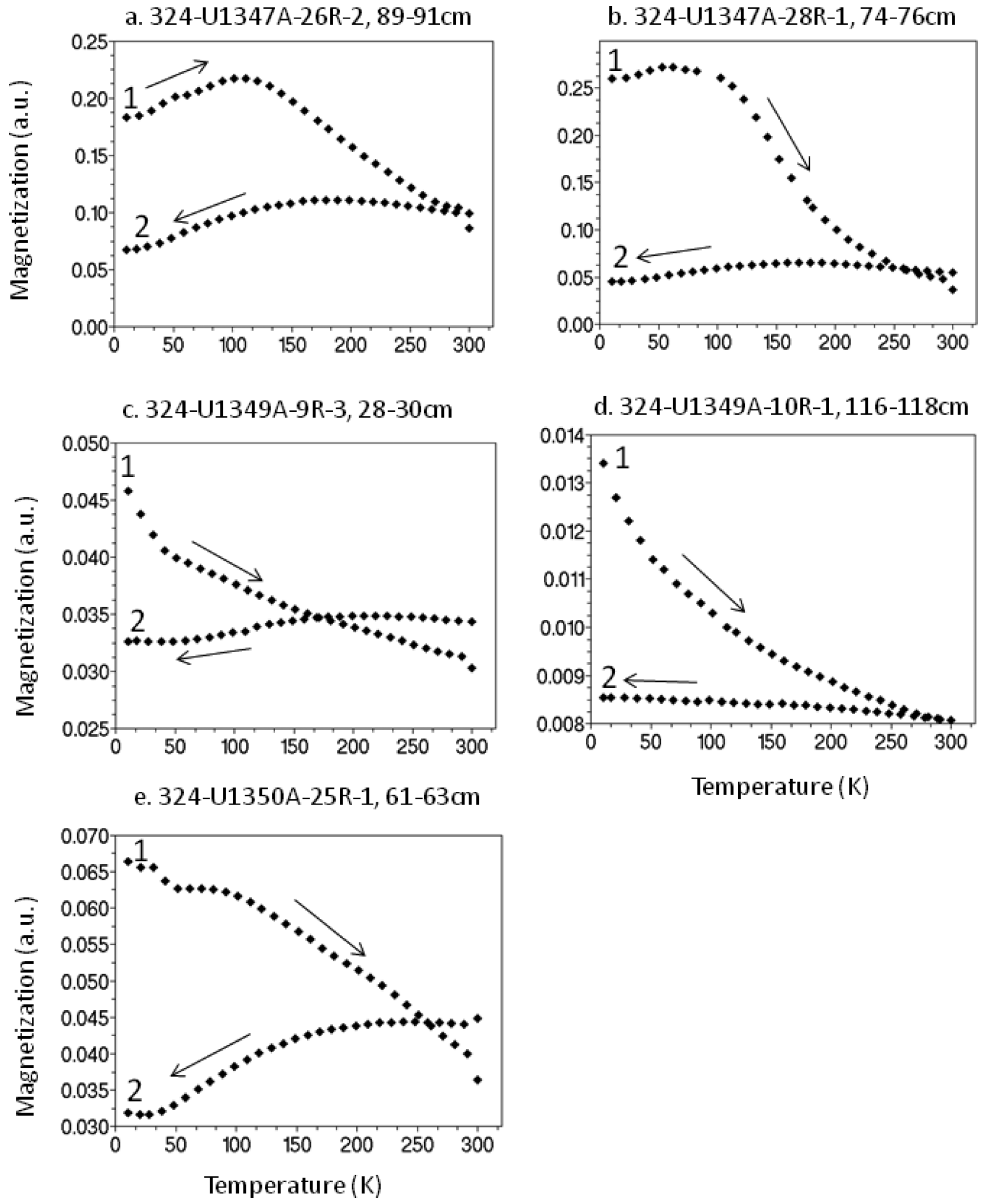

Figure 4. Temperature dependence of saturation remanence (SIRM) produced by a 2.5 T field. The curves labelled '1' show the zero-field warming curve from 20 to 300 K. The curves labelled '2' show the zero-field cooling (300–20 K) curve for SIRM produced at 300 K.

little with cooling, the shape of the SIRM demagnetization curve is very similar to that of synthetic titanomagnetite of composition x = 0.6 (Moskowitz *et al.* 1998).

Samples from Hole U1349A also display two different behaviours: one was observed for three samples (for example Sample 324-U1349A-9R-3, 28–30 cm, Fig. 4c): the room-temperature SIRM cooling curve shows a very small Verwey transition, more or less broad depending on the sample, which decreases the magnetization by no more than 10 per cent; the low-temperature SIRM decreases sharply at low temperature, then almost linearly, down to about two-thirds of the SIRM at 10 K. This could indicate the presence of a superparamagnetic (SP) fraction, whose magnetization is blocked at low temperature and unblocks with heating. Another, slightly different behaviour is observed in the other five measured samples (e.g. Sample 324-U1349A-10R-1, 116–118 cm, Fig. 4d): the room-temperature SIRM is almost constant with cooling, no transition is observed and the low-temperature SIRM decreases almost exponentially to about half its original value, showing again the presence of SP grains.

All the samples from Hole U1350A have a similar behaviour. A typical example is Sample 324-U1350A-25R-1, 61–63 cm (Fig. 4e): the room-temperature SIRM decreases by two-thirds through a broad transition centred around 120 K. The low temperature SIRM decreases through a small transition at 45 K and then drops almost linearly between 100 and 300 K to reach a value about half the original low-temperature SIRM. This small transition could be caused by the presence of ilmenite (Ishikawa 1962). The rest of the SIRM demagnetization curve is very similar to that of synthetic titanomagnetite of composition $x = 0.6$ (Moskowitz *et al.* 1998).

3.3 Susceptibility versus temperature

Low-field susceptibility versus temperature curves (k–T curves) were measured to test the stability of the Fe-Ti oxides upon heating and to determine the Curie temperature. They were performed at low- and high-temperatures with the cryostat apparatus CS-L and the furnace CS-3 under Argon atmosphere coupled to the KLY-3 Kappabridge instrument (Agico, Czech Republic) at the University of Montpellier. For this experiment, bulk rock samples have been reduced to powder in an agate mortar and sieved to obtain 0.4–0.8 mm size fractions. At least one sample per flow was heated first from the liquid nitrogen temperature (78 K) to 900 K and cooled down to room temperature. In some cases, the low-temperature measurements were repeated by heating again from 78 K up to room temperature. The raw susceptibility data were corrected for the empty sample holder and normalized to the maximum susceptibility.

U1347: 6 samples were measured and they showed 3 different behaviours. Although they all have rather low Curie temperatures between 150 and 250°C, they showed various degrees of reversibility. The susceptibility increases strongly from low-temperature to the Curie temperature and then decreases very sharply. Sample 324-U1347A-28R-1, 5–7 cm (Fig. 5a) is almost perfectly reversible. This indicates the presence of homogeneous Ti-rich titanomagnetites (Kontny *et al.* 2003; Camps *et al.* 2011). According to these previous studies, this type of curve also corresponds to samples that are predominantly MD at room temperature, but the FORC measurements for these samples are rather characteristic of PSD grain size. Sample 324-U1347A-27R-5, 12–14 cm (Fig. 5b) seems to transform into a titanomagnetite with a higher Curie temperature (i.e. lower titanium content) when heated. Finally, sample 324-U1347A-26R-2, 89–91 cm (Fig. 5c) shows a complex mineralogy: two components are visible upon cooling after heating to 450°C and the susceptibility is strongly irreversible after subsequent heating to 550°C.

U1349: Two different types of behaviours can be identified in the k–T curves of samples from this site. The first type, in the samples from the top-most part of the flow, is characterized by a mostly reversible susceptibility with heating and a high Curie temperature, close to that of pure magnetite (Fig. 5d). Similar curves were measured by Kontny *et al.* (2003) and Camps *et al.* (2011) on lava flows from Hawaii and Iceland, respectively; the presence of magnetite can be interpreted as resulting from high-temperature oxidation. It is also possible that the high Curie temperature values are caused by the presence of titanohematite produced by high-temperature deuteritic oxidation. A common feature of all these samples is a reddish colour.

The second behaviour, observed in samples from the bottom part of the flow, shows the presence of two Curie temperatures (Fig. 5e). One Curie temperature value is around 380°C, more or less pronounced, and is indicative of Ti-rich titanomagnetite(-maghemite). The other Curie temperature is around 550°C and is indicative of Ti-poor titanomagnetite. Upon cooling, only the highest Curie temperature remains and the component with the lowest Curie temperature completely disappears. As a result, the curve is strongly irreversible, with a final susceptibility that is about one half of the initial susceptibility. This behaviour could be caused by the inversion of small grains of the low-temperature titanomaghemite phase into haematite when the temperature increases.

U1350: The kT curves display a range of different behaviours, but the main features are similar to the type 1a/2 from Kontny *et al.* (2003): two Curie temperatures are present upon heating, indicating the presence of two magnetic phases. After heating, only one Curie temperature remains. The three Curie temperatures can be all very close (Fig. 5f), and the irreversibility can be marked (Figs 5g and h).

4 PALAEOINTENSITY DETERMINATIONS

4.1 Methods

Palaeointensity determinations were carried out in Montpellier laboratory following the classical Thellier & Thellier (1959) method. The samples were heated and cooled twice at each temperature step T_i. During the cooling phase, a 35-μT induction field was applied along the cylinder axis of the specimens (z-axis) for the first cycle and in the opposite direction for the second one. Samples were divided into two batches to allow for different heating steps chosen according to the sample thermomagnetic behaviour. The first batch contained all the samples from Hole U1349A and about half the samples from Hole U1350A. Sixteen temperature steps up to 625°C were carried out with increments of 150°C up to 300°C and then of 25°C up to 625°C. The second batch contained all the samples from Hole U1347A and the rest of the samples from Hole U1350A. They were subjected to 13 heating steps with increments depending on their thermal behaviour. To detect alteration of the TRM spectrum as the laboratory heating temperature is progressively increased, this double-heating protocol is accompanied with a sliding pTRM check procedure (Prévot *et al.* 1985). The principle is to reinvestigate the pTRM capacity in a given temperature interval after heating to higher temperature. Here we remeasured, throughout the whole experiment, the pTRM intensity acquired in a temperature interval from T_{i-2} to room temperature after heating at T_i.

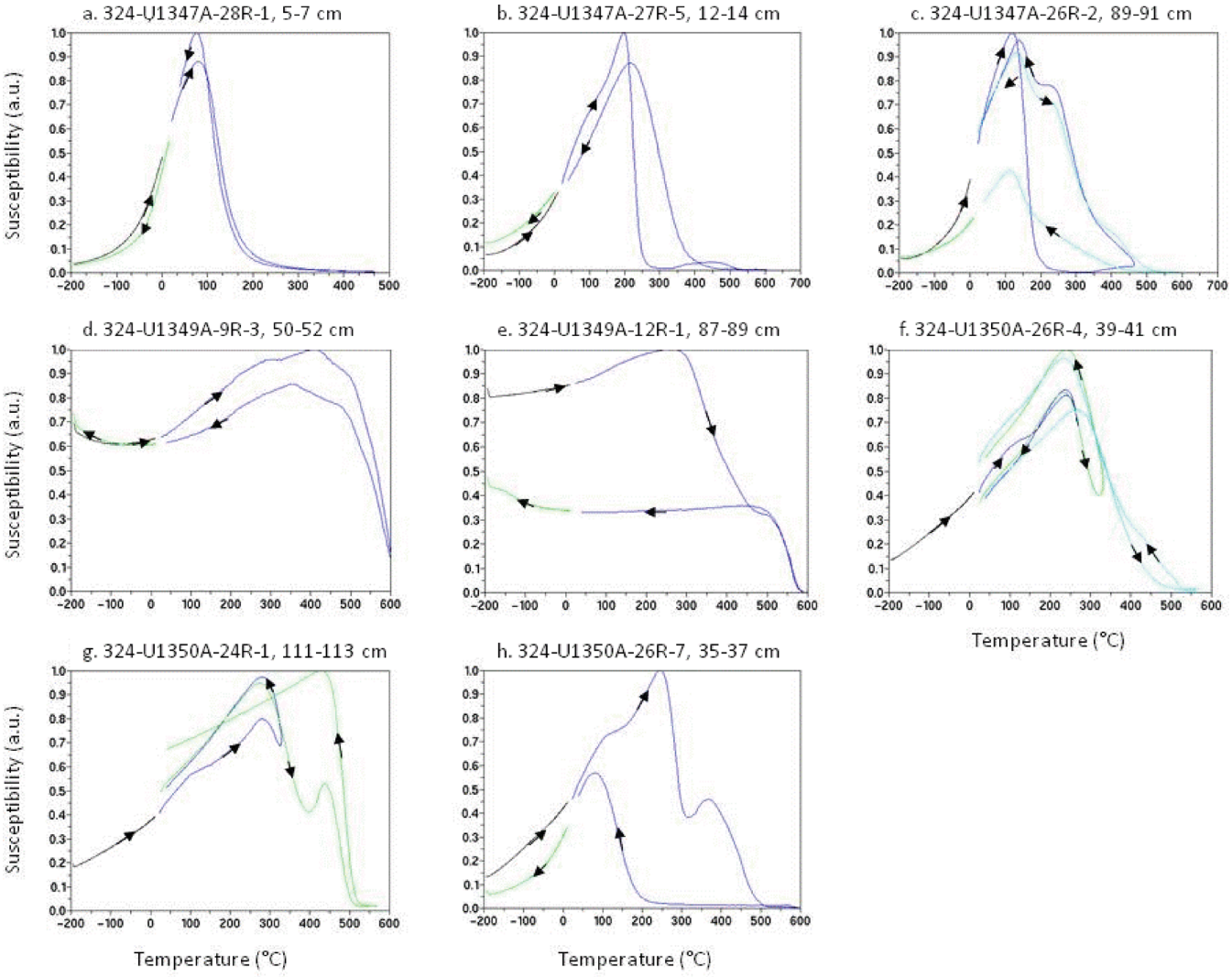

Figure 5. Representative examples of low-field susceptibility versus temperature (k–T) curves. Heating and cooling curves are indicated with the arrows.

All heating–cooling cycles were performed under a vacuum better than 10^{-2} Pa to limit possible oxidation during experiment. Each heating-cooling cycle required between 7 and 10 hr. The temperature reproducibility between heating runs at the same temperature step is within 1°C. This control is ensured by means of three thermocouples placed at different positions within the heating chamber, plus three others sealed inside three dummy samples. The intensity of laboratory magnetic field is held with a precision better than 0.1 μT. The remanence was measured after each heating-cooling cycle at room temperature with a JR-5A spinner magnetometer.

4.2 Selection criteria

The representation and statistical analysis of palaeointensity data were carried out with the ThellierTool software provided by Leonhardt *et al.* (2004). In this software, the basic statistical parameters are those introduced by Coe *et al.* (1978) with the modifications proposed by Prévot *et al.* (1985).

We adopted a standard set of strict criteria derived from those of Selkin & Tauxe (2000) and Plenier *et al.* (2003) to interpret the individual palaeointensity data and screen out those of poor quality. These criteria are based on three considerations:

(1) NRM–TRM diagrams: Palaeointensity measurements were represented and analysed by means of an Arai diagram in which the NRM remaining is plotted against the TRM acquired after each pair of heating experiments (Nagata *et al.* 1963). The slope of the least-squares-fit line computed from the linear part of these plots gives an estimate of the palaeointensity. A palaeointensity value is rejected when the least-squares segment is defined by less than four points ($n < 4$) or it spans less than 30 per cent of the total NRM ($f < 0.3$).

(2) pTRM checks : It is now widely accepted that a linear part on NRM–TRM diagram is not a proof by itself of the absence of alteration in the TRM spectrum during the Thellier experiment. Hence, pTRM checks must be performed to assess the reliability of a palaeointensity estimate. We quantified the difference between two pTRM acquisitions at the same temperature by means of the Difference Ratio (DRAT) parameter (Selkin & Tauxe 2000). DRAT is expressed in percent and corresponds to the maximum difference measured between repeated pTRM acquisition measurements normalized by the length of the selected NRM–TRM segment. A maximum acceptable threshold is fixed arbitrarily at 10 per cent.

(3) Vector endpoint diagrams: Jointly, we checked on the directional plots computed from the palaeointensity experiments that the NRM fraction used to calculate the palaeointensity corresponds

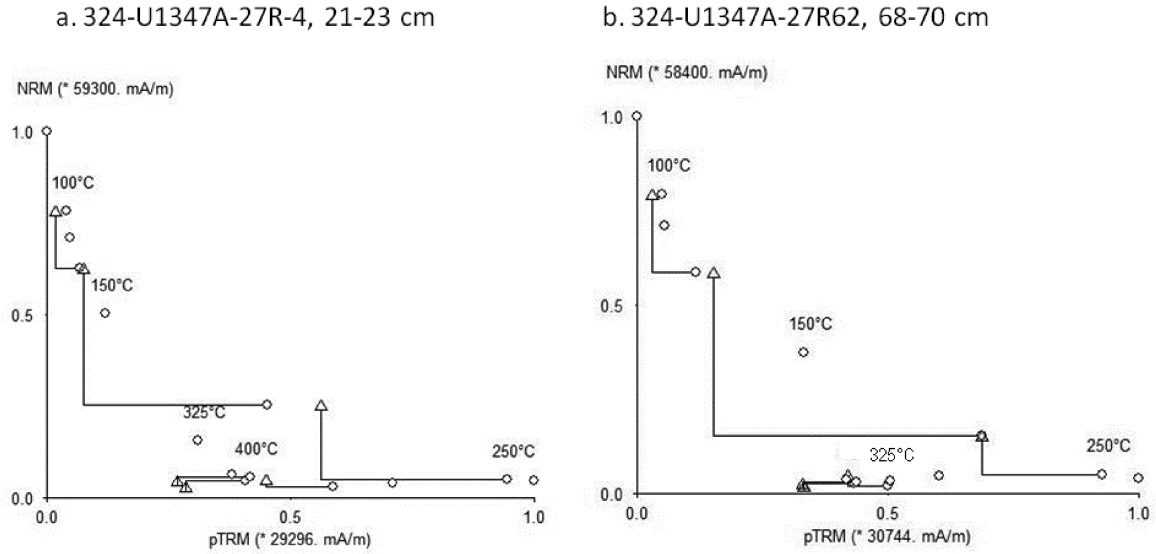

Figure 6. Examples of Arai plots of two samples from Hole U1347A. Arai plots are strongly concave-up, leading to the rejection of all the palaeointensity estimates from samples from this hole. (a) Sample 324-U1347A- 27R-4, 21–23 cm: (b) Sample 324-U1347A- 27R-2, 68–70 cm. The plots show the normalized amount of magnetization, pTRM, acquired at each heating step.

effectively to the ChRM of the core. The low-temperature part of the NRM may contain natural secondary magnetizations, and spurious remanent magnetization acquired during laboratory heating may be superimposed on the NRM if chemical changes in the magnetic minerals occurred. This check is achieved qualitatively by a visual inspection of the vector endpoint diagrams obtained during the Thellier–Thellier experiment. The points in the selected interval should trend towards the origin if the NRM is the ChRM. Moreover, the Maximum Angular Deviation (MAD) must be less than 5° on the selected temperature interval.

4.3 Results

4.3.1 Hole U1347A

The 15 samples all present the same characteristics: the Arai diagram is strongly concave-up (Fig. 6), which usually indicates the presence of MD grains. As expected from the thermomagnetic curves, nearly all the magnetization is destroyed after heating to 250°C. Moreover, most pTRM checks are negative with DRATs larger than 15 per cent. At first sight, this result is not consistent with the FORC diagrams, that point to SD grains. However, it is possible that the concave-up shape could be caused by magnetostatic interactions and/or alteration effects taking place during the numerous heatings. Although the contribution of intergrain magnetostatic interactions has never been quantified rigorously, and it is still debated if interacting SD grains have an effect on Thellier's laws (Shcherbakov *et al.* 1995; Shcherbakov & Sycheva 1997; Fabian 2001, Dunlop *et al.* 2005), this behaviour is not a good sign for reliability. However, it has to be noted that if the Arai diagram were linear, the potential presence of interactions should not have an effect on the pelaeointensity estimate, because the interactions should stay constant between the TRM acquired in the lab and the primary NRM. The presence of an important fraction of small SD particles close to the SP range at room temperature, which introduces a viscous component of magnetization, could also have this effect, though no SP behaviour was detected on FORC diagrams. As a result of this behaviour, none of the palaeointensity determinations on samples from Hole U1347A can be considered as reliable.

4.3.2 Hole U1349A

Eight out of 22 samples, from two different subunits, gave results with an excellent technical quality (Figs 7a and b). Most of the magnetization loss occurs at high temperature, between 375 and 575°C. Arai plots are very linear and pTRM checks are satisfied. Moreover, Zijderveld diagrams are reasonably linear and point to the origin of the diagram. As a result, q factors are quite high (all above 8). Palaeointensity values are between 16.7 and 21.4 μT (Table 1).

Some results are again concave-up (Figs 8a and b). They correspond to the irreversible thermomagnetic curves composed of two components, which are also the samples with the largest FWHM on the FORC diagram. The failure of these samples could be attributed to the presence of magnetostatic interactions.

4.3.3 Hole U1350A

These samples were subjected to different temperature steps because they were in two different batches. According to the thermomagnetic curves that showed some irreversibility after heating over 350°C, Arai diagrams are more or less linear up to about that temperature and display an erratic behaviour afterwards, probably because of magnetochemical transformations (Figs 9a and b). This low-temperature component could be used as a reliable palaeointensity estimate but none of the NRM demagnetizations point towards the origin of the Zijderveld diagrams on that temperature interval, even though MAD values are lower than 5°. Therefore, none of the results from Hole U1350A were considered as reliable.

4.3.4 Final results

In the end, only nine samples from three different flows, all from Hole U1349A, give a reliable palaeointensity estimate. The results as well as the various Thellier–Thellier parameters are summarized in Table 1. The palaeointensity values are similar with values ranging between 16.7 and 21.4 μT. The averages per flow are 19.4 μT

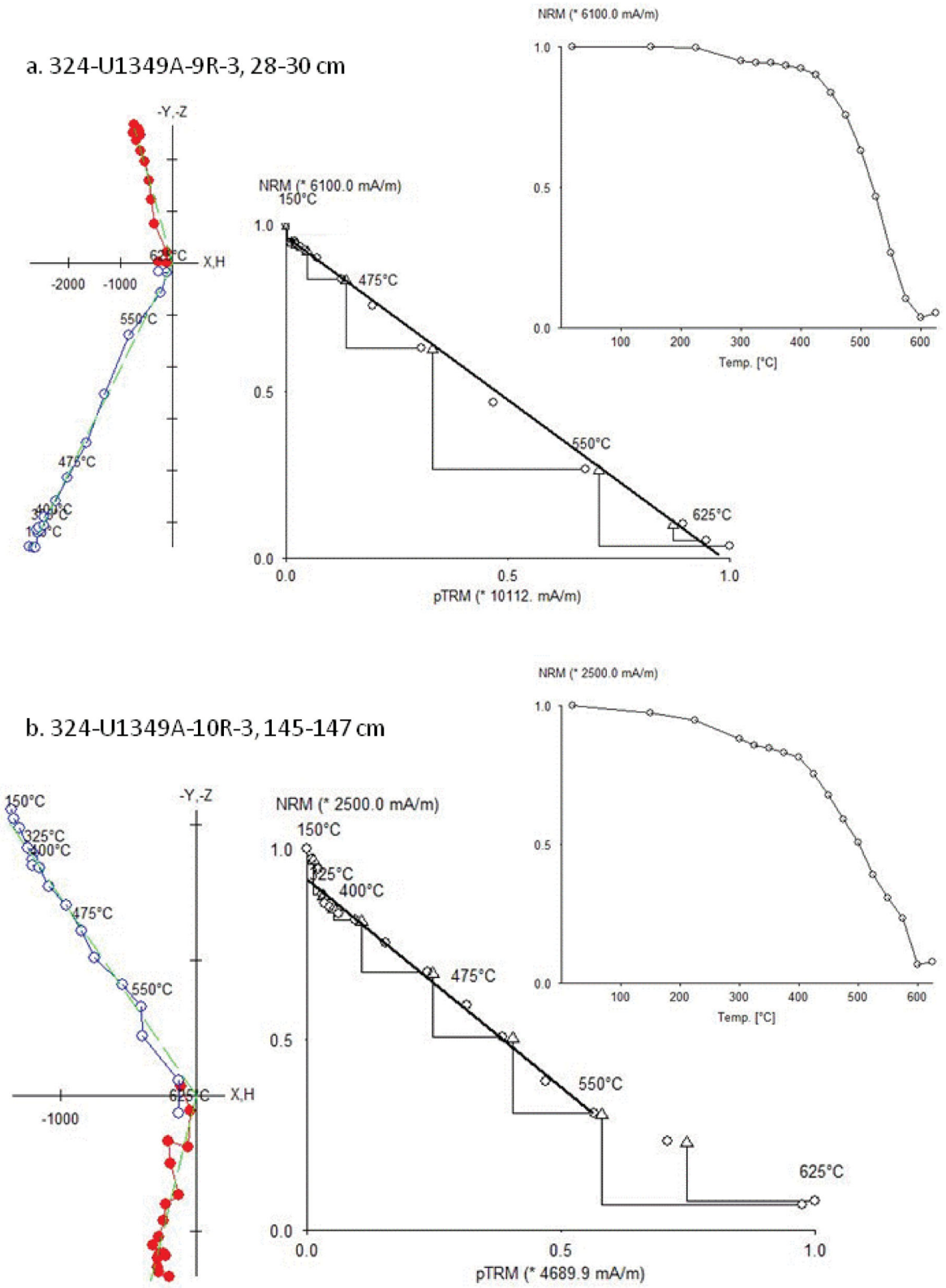

Figure 7. Examples of Arai plots, Zijderveld diagrams and demagnetization spectra for two samples from Hole U1349A that give apparently reliable palaeointensity determinations. (a) Sample 324-U1349A-9R-3, 28–30 cm; (b) Sample 324-U1349A-10R-3, 145–147 cm. Three plots are shown for each sample. The Zjiderfeld (orthogonal vector) plot (on left-hand panel) shows magnetization vector endpoints projected on horizontal and vertical planes at each demagnetization step. Closed circles indicate the projection on the vertical plane whereas open circles indicate the horizontal plane. The Arai plot (middle panel) is as in Fig. 6. Demagnetization spectra plot (right-hand panel) shows the normalized amount of magnetization intensity remaining after each demagnetization step.

Table 1. Palaeointensity results for the nine successful samples. T range: temperature range used to calculate the palaeointensity estimate; n: number of points used on the best fit line; f: fraction of NRM used to calculate the palaeointensity estimate; g: gap factor (Coe *et al.* 1978); q: quality factor (Coe *et al.* 1978). The field values are given with their standard deviation. The weighted average field is calculated using the quality factor as a weight; the average VDM is calculated using the weighted average palaeointensity values.

Sample name	T range (°C)	n	f	g	q	Field ± σ (μT)	Av. Field (μT)	Weighted av. Field (μT)	VDM ($\times 10^{22}$ Am^2)
324-U1349A-9R-2,104–106 cm	225–600	14	0.97	0.89	47.84	16.7 ± 0.3			
324-U1349A-9R-3,28–30 cm	225–575	13	0.92	0.83	33.54	21.4 ± 0.5			
324-U1349A-9R-3,50–52 cm	225–550	12	0.65	0.82	13.85	21.7 ± 0.8	19.4	18.5	4.9
324-U1349A-10R-1,96–98 cm	225–550	12	0.74	0.87	21.05	19.4 ± 0.6			
324-U1349A-10R-1,116–118 cm	225–550	12	0.67	0.87	19.61	20.6 ± 0.6			
324-U1349A-10R-3,22–24 cm	225–550	12	0.66	0.88	18.33	17.8 ± 0.6			
324-U1349A-10R-3,110–112 cm	225–500	10	0.55	0.86	8.97	19.0 ± 1.0			
324-U1349A-10R-3,145–147 cm	225–550	12	0.67	0.88	18.12	20.3 ± 0.7	19.4	19.4	5.1
324-U1349A-13R-6,31–33 cm	325–500	8	0.41	0.85	8.67	18.8 ± 0.8	18.8	18.8	4.8

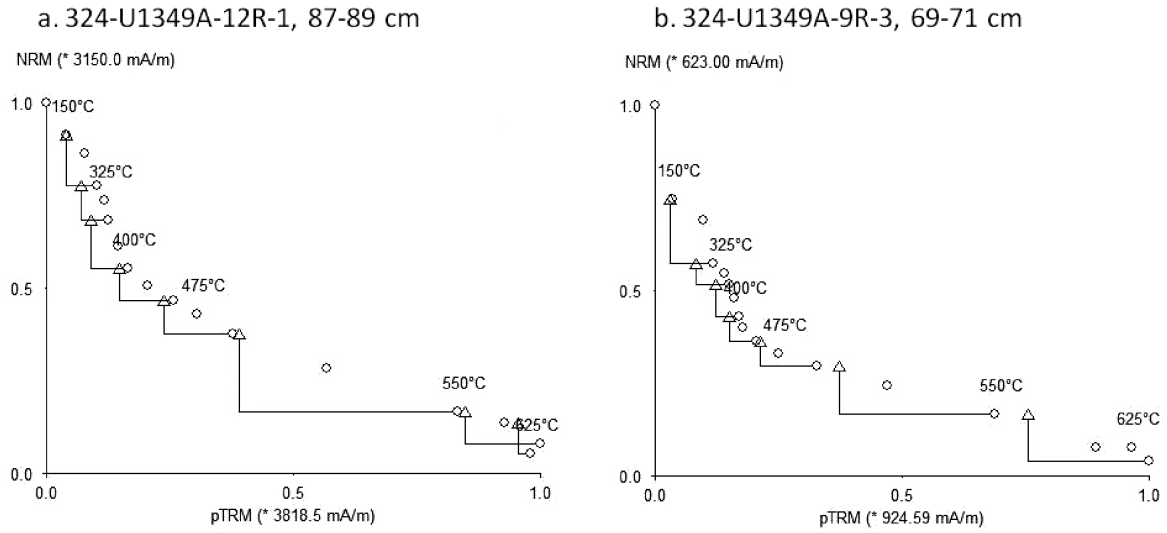

Figure 8. Examples of Arai plots for two samples from Hole U1349A that did not yield reliable palaeointensity determinations because of a concave-up shape of the Arai plot. (a) Sample 324-U1349A-12R-1, 87–89 cm; (b) Sample 324-U1349A-9R-3, 69–71 cm.

for two of them and 18.8 μT for the third one. We also calculated the weighted averages where w is the parameter w = (f.g)/s, f the fraction of NRM destroyed on the temperature range used for the palaeointensity determination, g the gap factor and s the standard deviation (Coe *et al.* 1978; Prévot *et al.* 1985). The weighted averages of the palaeointensities are then 18.5, 19.4 and 18.8 μT for the three flows. The remarkably consistency between values is another argument towards the reliability of these measurements.

5 DISCUSSION

5.1 Magnetic properties

As expected in old rocks that have lain beneath the sea for many tens of millions of years, magnetic properties show a wide range of complex behaviour. According to the various magnetic measurements that we carried out (including palaeointensity measurements), the results can be summarized and the success/failure of palaeointensity experiments could tentatively be explained in the following way:

(1) Hole U1347A: According to FORC measurements, the magnetic carriers are SD particles with some interactions. Low-temperature and susceptibility versus temperature measurements point to titanomagnetite $Fe_{3-x}Ti_xO_4$ with $x = 0.6$, with another non-reversible phase in some samples. Unfortunately, none of the palaeointensity results can be considered as reliable, because of the concave-up shape of the Arai diagrams. This could have several causes: the presence of magnetostatic interactions, as suggested by the FORC diagrams; the presence of an important SP component; or the chemical and structural alterations taking place during the thermal treatments (Fig. 5b). Since all heatings and coolings are performed in the presence of the external field, the alterations can give rise to a CRM and a distortion of the blocking spectra (Kosterov & Prévot 1998; Yamamoto *et al.* 2003).

(2) Hole U1349A: About half the samples from Hole U1349A gave high quality palaeointensity determinations, with linear Arai plots and Zijderveld diagrams on almost the whole demagnetization spectrum. The magnetization seems to be stable upon heating up to 575°C. The susceptibility versus temperature curves are mostly reversible, with a high Curie temperature, and the low temperature curves show a broad Verwey transition. All these

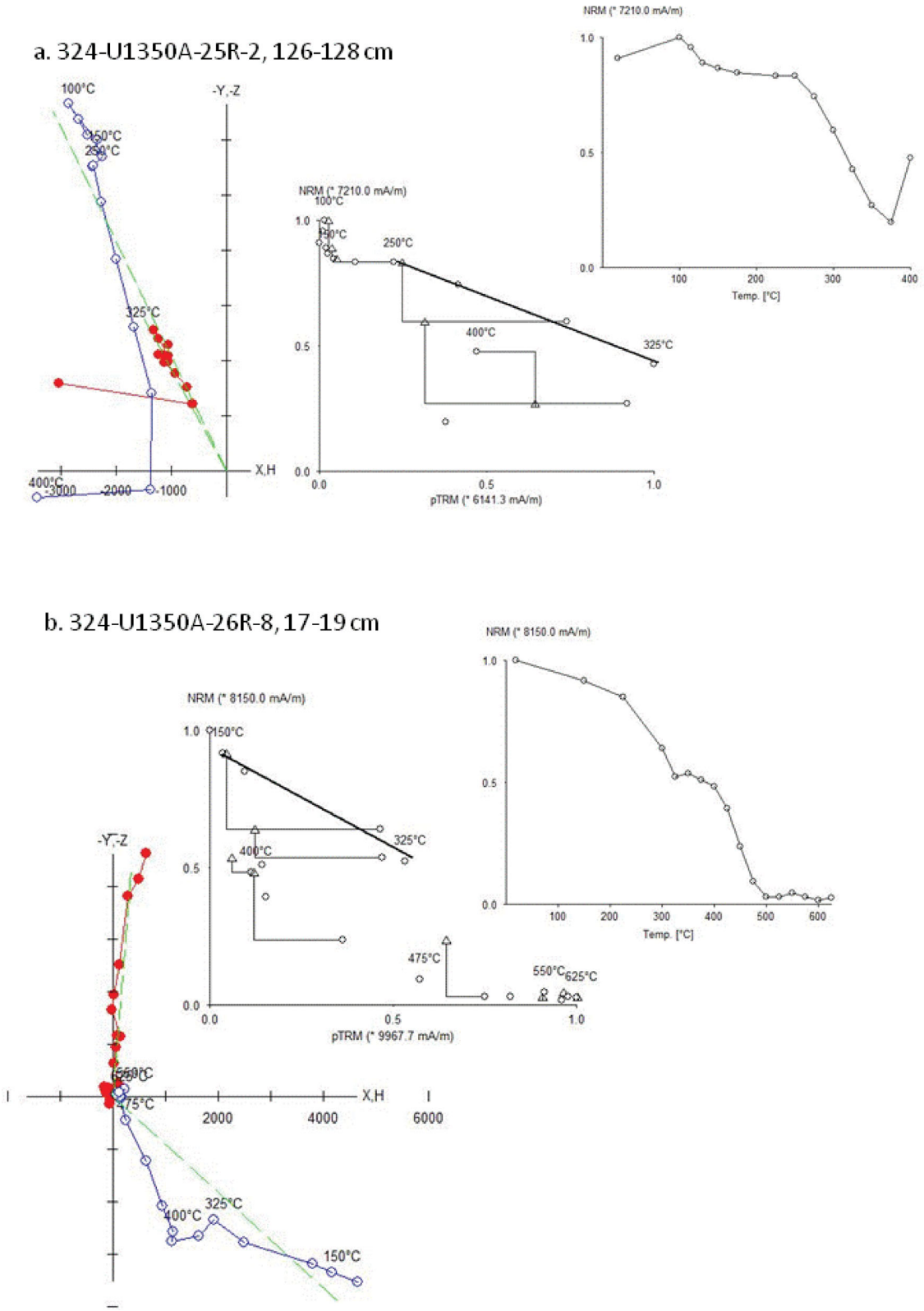

Figure 9. Examples of Arai plots, Zijderveld diagrams and demagnetization spectra for two samples from Hole U1350A that did not give a reliable palaeointensity estimate. (a) Sample 324-U1350A-25R-2, 126–128 cm; (b) Sample 324-U1350A-26R-8, 17–19 cm.

measurements point to the presence of low-Ti titanomagnetite. The samples that failed the palaeointensity experiments (mostly because of a strongly curved Arai diagram) do not have a reversible k–T curve.

(3) Hole U1350A: these samples have the most complex mineralogy. According to both the palaeointensity behaviour and the k–T curves, two components are present. However, the low-temperature component does not seem to be a primary magnetization, and the

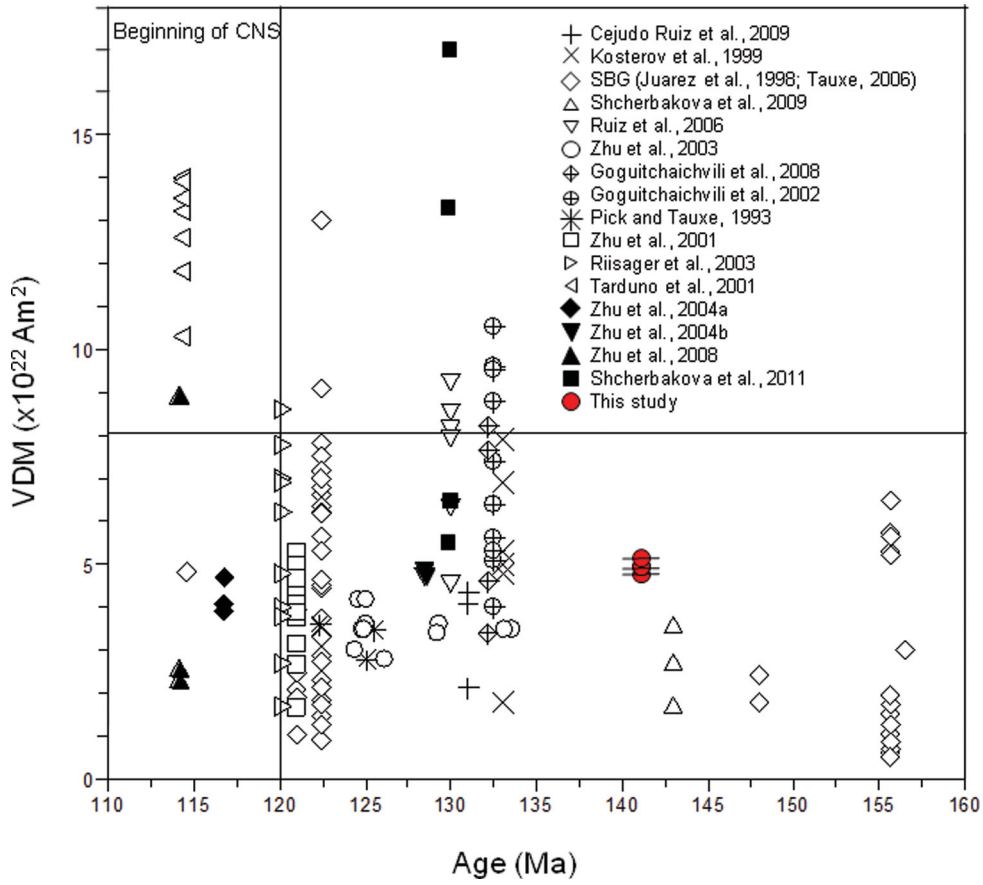

Figure 10. Summary of the VDM data in the 125–160 Ma time range. Available data from the PINT database (Biggin *et al.* 2010) are plotted together with data from this study. The present-day VDM is shown as a line at 8×10^{22} Am^2. See references Pick and Tauxe 1993; Juarez *et al.* 1998; Kosterov *et al.* 1999; Tarduno *et al.* 2001; Goguitchaichvili *et al.* 2002, 2008; Riisager *et al.* 2003; Tauxe 2006; Cejudo Ruiz *et al.* 2009; Ruiz *et al.* 2009; Shcherbakova *et al.* 2009, 2011; Zhu *et al.* 2001, 2003, 2004a,b, 2008.

high-temperature could be a product of alteration due to the laboratory heating. The unblocking temperatures are difficult to calculate because of the alteration taking place around 400°C, but they seem to be higher than those of Hole U1347A and lower than those from Hole U1350A. Only a very broad low-temperature transition could be identified. All these measurements could indicate the presence of titanomagnetite and titanomaghemite with various x and z parameters.

The choice of the thresholds for selection criteria in Thellier experiments is somewhat subjective. In our experiments, the subjective choices are not critical because all the accepted palaeointensity results are of very high quality. All the parameters indicating the quality of the determination are well above the chosen limits. Moreover, the consistency of the nine determinations is a good indication that our palaeointensity estimates are reliable.

There remains the question of the reddish colour observed in most of our samples from Hole U1349A that suggests the presence of haematite. Also, in both shipboard and on-shore AF demagnetizations carried out at Doshisha University, Kyoto, 10 to 25 per cent of the NRM could not be demagnetized after 100 mT. According to the rock magnetic measurements, no haematite was identified, whether through the Morin transition, or through the presence of very high coercivity grains on the FORC diagrams. Moreover, the Arai and Zijderveld diagrams clearly show only one component of magnetization that points towards the origin of the diagram. If haematite is present, it does not seem to carry any magnetization, or at least a negligible fraction compared to that of the main magnetization carrier, which is probably close to magnetite.

5.2 VDM values

Palaeointensity values must be converted into VDM to be compared with data from other locations, using the inclination measured at this site. The directions obtained from the palaeointensity experiments show a very large scattering, and the averaging is not sufficient. Therefore we prefer to use inclinations measured from shore-based thermal and alternating-field demagnetizations at Doshisha University, Kyoto. We obtain weighted averages VDM values of 4.9, 5.1 and 4.8×10^{22} Am^2, respectively, for each of the three lava flows. We can compare these values with other values obtained only with the Thellier–Thellier method, from the PINT database (Biggin *et al.* 2010). When plotting all the available data dated between 110 and 160 Ma (which, therefore, includes the beginning of the Cretaceous Normal Superchron) it is obvious that there is a very large discrepancy in between data from rocks of the same age range, and even within the same study (Fig. 10). For the data within the CNS, this has been explained by the fact that the secular variation could be stronger during this quiet period. However, for the data just before the CNS (120 Ma and older), most studies from whole-rock samples give data that are consistent and low (Pick & Tauxe 1993;

Zhu *et al.* 2001, 2003, 2004b; Riisager *et al.* 2003; Shcherbakova *et al.* 2009). On the other hand, studies from submarine basaltic glass (SBG; Juarez *et al.* 1998; Tauxe 2006), those from the Mexico group as well as Kosterov *et al.* (1997) give much more scattered VDM values, some of which being much higher than those from the previously cited studies, and even higher than the present-day VDM. This is partly explained by the palaeosecular variation which cannot be always adequately averaged in palaeointensity experiments. Our study, however, gives VDM values that are consistent within a flow unit and between flows. Our values are lower than the present day VDM (around 8×10^{22} Am^2), which tends to support the hypothesis of a Mesozoic Dipole Low. However, they are not as low as the values measured by Shcherbakova *et al.* (2009), Zhu *et al.* (2003) and Cejudo Ruiz *et al.* (2009).

6 CONCLUSION

1. Thellier–Thellier palaeointensity determinations on 60 submarine samples from Shatsky Rise (145 Ma) gave 9 high-quality, consistent and reliable palaeointensity values.

2. Magnetic properties show that in most cases, the magnetic signal is carried by a complex assemblage of single-domain titanium iron oxide grains.

3. The VDM values calculated from these palaeointensity values are around 5×10^{22} Am^2. These values are consistent with the hypothesis of a Mesozoic Dipole Low.

ACKNOWLEDGMENTS

This research used samples and data provided by the Integrated Ocean Drilling Program (IODP). We thank Yohan Guyodo and France Lagroix for helpful discussions and for help using the MPMS. The MPMS XL5 EverCool system at IPGP was financed by the Conseil Régional d'Ile-de-France (N°I-06–206/R), INSU-CNRS, IPGP and ANR (N°06-JCJC-0144). We thank Carlo Laj and Catherine Kissel for access to the AGM at LSCE, Gif-sur-Yvette. We thank Valera Shcherbakov, Andrew Biggin and an anonymous reviewer for their reviews and helpful comments.

REFERENCES

Biggin, A.J., McCormack, A. & Roberts, A., 2010. Palaeointensity database updated and upgraded, *Eos,* **91,** 15, doi:10.1029/2010EO020003.

Camps, P., Singer, B., Carvallo, C., Goguitchaichvili, A., Fanjat, G. & Allen, B., 2011. The Kamikatsura event and the Matuyama–Brunhes reversal recorded in lavas from Tjörnes Peninsula, northern Iceland, *Earth planet. Sci. Lett.,* **310,** 33–44.

Carvallo, C., Roberts, A.P., Leonhardt, R., Laj, C., Kissel, C., Perrin, M. & Camps, P., 2006. Increasing the efficiency of palaeointensity analyses by selection of samples using first-order reversal curve diagrams, *J. geophys. Res.,* **111,** B12 103, doi:10.1029/2005JB004126.

Carvallo, C. & Camps, P., in press. Data report: Magnetic properties of basalts from Shatsky Rise, eds Sager, W.W., Sano, T. & Geldmacher, J., and the Expedition 324 Scientists, Proc. IODP, 324: Tokyo (Integrated Ocean Drilling Program Management International, Inc.).

Cejudo Ruiz, R., Goguitchaichvili, A., Morales, J., Trindade, R.I.F., Alva Valdivia, L.M. & Urrutia-Fucugauchi, J., 2009. Absolute Thellier paleointensities from Ponta Grossa dikes (southern Brazil) and the early Cretaceous geomagnetic field strength, *Geofisica Internacional,* **48,** 243–252.

Coe, R.S., Grommé, S. & Mankinen, E.A., 1978. Geomagnetic paleointensities from radiocarbon-dated lava flows on Hawaii and the question of the Pacific nondipole low, *J. geophys. Res.,* **83,** 1740–1756.

Dunlop, D.J., Zhang, B.X. & Özdemir, Ö., 2005. Linear and nonlinear Thellier paleointensity behavior of natural minerals, *J. geophys. Res.,* **110,** B01 103, doi:10.1029/2004JB003095.

Fabian, K., 2001. A theoretical treatment of paleointensity determination experiments on rocks containing pseudo-single or multi-domain magnetic particles, *Earth planet. Sci. Lett.,* **188,** 45–58.

Goguitchaichvili, A., Alva-Valdivia, L.M., Urrutia, J., Morales, J. & Ferreira Lopes, O., 2002. On the reliability of Mesozoic Dipole Low: new absolute palaeointensity results from Parana Flood Basalts (Brazil), *Geophys. Res. Lett.,* **13,** doi:10.1029/2002GL015242.

Goguitchaichvili, A., Cejudo Ruiz, R., Sanchez Bettucci, L., Aguilar Reyes, B., Alva-Valdivia, L.M., Urrutia-Fucugauchi, J., Morales, J. & Calvo Rathert, M., 2008. New absolute palaeointensity results from the Parana Magmatic Province (Uruguay) and the Early Cretaceous geomagnetic paleofield, *Geochem. Geophys. Geosyst.,* **9,** doi:10.1029/2008GC002102.

Ishikawa, Y., 1962. Magnetic properties of Ilmenite-Hematite system at low temperatures, *J. Phys. Soc. Japan.,* **17**(suppl. B1), 239–243.

Juarez, M.T., Tauxe, L., Gee, J.S. & Pick, T., 1998. The intensity of the Earth's magnetic field over the past 160 million years, *Nature,* **394,** 878–881.

Kontny, A., Vahle, C. & De Wall, H., 2003. Characteristic magnetic behavior of subaerial and submarine lava units from the Hawaiian scientific drilling project (hsdp-2), *Geochem. Geophys. Geosyst.,* **4,** 2, doi:10.1029/2002GC000304.

Kosterov, A.A. & Prévot, M., 1998. Possible mechanisms causing failure of Thellier palaeointensity experiments in some basalts, *Geophys. J. Int.,* **134,** 554–572.

Kosterov, A.A., Prévot, M., Perrin, M. & Shashkanov, V.A., 1997. Palaeointensity of the Earth's magnetic field in he Jurassic: new results from a Thellier study of the Lesotho Basalt, south Africa, *J. geophys. Res.,* **102,** 24 859–24 872.

Kosterov, A.A., Perrin, M., Glen, J.M. & Coe, R.S., 1998. Palaeointensity of the Earth's magnetic field in Early Cretaceous times : the Paraná Basalt, Brazil, *J. geophys. Res.,* **103,** 9739–9753.

Leonhardt, R., Heunemann, C. & Krása, D., 2004. Analysing absolute palaeointensity determinations: acceptance criteria and the software Thelliertool4.0, *Geochem. Geophys. Geosyst.,* **5**(12), doi:10.1029/2004GC000807.

Levi, S., 1977. The effect of magnetite particle size on paleointensity determinations of the geomagnetic field, *Phys. Earth planet. Inter.,* **13,** 245–259, doi:10.1016/0031-9201(77)90107-8.

Mahoney, J.J., Duncan, R.A., Tejada, M.L.G., Sager, W.W. & Bralower, T.J., 2005. Jurassic–Cretaceous boundary age and mid-ocean-ridge–type mantle source for Shatsky Rise, *Geology,* **33**(3), 185–188.

Moskowitz, B.M., Jackson, M. & Kissel, C., 1998. Low temperature behaviour of titanomagnetites, *Earth planet. Sci. Lett.,* **157,** 141–149.

Nagata, T., Arai, Y. & Momose, K., 1963. Secular variation of the geomagnetic total force during the last 5000 years, *J. geophys. Res.,* **68,** 5277–5281.

Nakanishi, M., Sager, W.W. & Klaus, A., 1999. Magnetic lineations within Shatsky Rise, northwest Pacific Ocean: implications for hot spot–triple junction interaction and oceanic plateau formation, *J. geophys. Res.,* **104,** 7539–7556.

Ogg, J.G. & Smith, A.G., 2004. The geomagnetic polarity timescale, in *A Geological Time Scale 2004,* pp. 63–86, eds Gradstein, F., Ogg, J. & Smith, A., Cambridge University Press, Cambridge, UK.

Perrin, M., Prévot, M. & Mankinen, E.A., 1991. Low intensity of the geomagnetic field in early Jurassic time, *J. geophys. Res.,* **96,** 14 197–14 210.

Perrin, M. & Shcherbakov, V., 1997. Paleointensity of the earth's magnetic field for the past 400 Ma: evidence for a dipole structure during the Mesozoic Low, *J. Geomag. Geoelectr.,* **49,** 601–614.

Pick, T. & Tauxe, L., 1993. Geomagnetic palaeointensities during the Cretaceous normal superchron measured using submarine basaltic glass, *Nature,* **366,** 238–242.

Pike, R.P., Roberts, A.P. & Verosub, K.L., 1999. Characterizing interactions in fine magnetic particle systems using first order reversal curves, *J. Appl. Phys.,* **85,** 6660–6667.

Plenier, G., Camps, P., Coe, R.S. & Perrin, M., 2003. Absolute palaeointensity of Oligocene (24–30 Ma) lava flows from the Kerguelen Archipelago (southern Indian Ocean), *Geophys. J. Int.,* **154,** 877–890.

Prévot, M., Mankinen, E.A., Coe, R.S. & Grommé, C.S., 1985. The Steens Mountain (Oregon) geomagnetic polarity transition. 2. Field intensity variations and discussion of reversal models, *J. geophys. Res.,* **90,** 10 417–10 448.

Prévot, M., Derder, M.M., McWilliams, M. & Thompson, J., 1990. Intensity of the Earth's magnetic field: evidence for a Mesozoic Dipole Low, *Earth planet Sci. Lett.,* **97,** 129–139.

Riisager, P., Riisager, J., Zhao, X. & Coe, R.S., 2003. Cretaceous geomagnetic paleointensities: Thellier experiments on Pillow lavas and Submarine basaltic glass from the Ontong Java Plateau, *Geochem. Geophys. Geosyst.,* **4,** 12, doi:10.1029/2003GC000611.

Roberts, A.P., Pike, C.R. & Verosub, K.L., 2000. FORC diagrams: a new tool for characterizing the magnetic properties of natural samples, *J. geophys. Res.,* **105,** 28 461–28 475.

Ruiz, R.C., Goguichaichvili, A., Geuna, S.E., Alva Valdivia, L.M., Sole, J. & Morales, J., 2006. Early cretaceous absolute geomagnetic paleointensities from Cordoba Province (Argentina), *Earth Planets Space,* **58,** 1333–1339.

Sager, W.W. & Han, H.-C., 1993. Rapid formation of the Shatsky Rise oceanic plateau inferred from its magnetic anomaly, *Nature,* **364,** 610–613.

Sager, W.W., Sano, T., Geldmacher, J. & the Expedition 324 Scientists, 2010. *Proceeding of the Integrated Ocean Drilling Program Management International, Inc. (IODP),* 324, Tokyo.). doi:10.2204/iodp.proc.324.2010.

Selkin, P.A. & Tauxe, L., 2000. Long term variations in palaeointensity, *Phil. Trans. R. Soc. A: Math. Phys. Eng. Sci.,* **358**(1768), 1065–1088.

Shcherbakov, V.P. & Sycheva, N.K., 1997. Fulfillment of the Thellier's laws of independence and additivity of partial thermoremanent magnetizations for interacting single-domain grains (numerical experiment), *Izvestiya, Phys. Solid Earth,* **4,** 83–88.

Shcherbakov, V.P., Lamash, B.E. & Sycheva, N.K., 1995. Monte-Carlo modelling of thermoremanence acquisition in interacting single domain grains, *Phys. Earth planet. Inter.,* **87,** 197–211.

Shcherbakova, V.V., Perrin, M., Shcherbakov, V.P., Pavlov, V.E., Ayvaz'yan, A. & Zhidkov, G.V., 2009. Rock magnetic and palaeointensity results from Mezosoic baked contacts of Armenia, *Earth Planets Space,* **61,** 23–39.

Shcherbakova, V.V., Kovalenko, D.V., Shcherbakov, V.P. & Zhidkov, G.V., 2011. Paleointensity of the geomagnetic field in the Cretaceous (from Cretaceous rocks of Mongolia), *Izvestiya, Phys. Solid Earth,* **47,** 775–791.

Shipboard Scientific Party, 2002. Leg 198 Summary, in *Proceedings of the ODP, Init. Repts.,* Vol. 198, pp. 1–148, eds Bralower, T.J., Premoli Silva, I. & Malone, M.J. [CD-ROM]. Available from: Ocean Drilling Program, Texas A&M University, College Station, TX 77845–9547, USA.

Smith, W.H.F. & Sandwell, D.T., 1997. Global seafloor topography from satellite altimetry and ship depth soundings, *Science,* **277,** 1956–1962.

Tarduno, J.A., Cottrell, R.D. & Smirnov, A.V., 2001. High geomagnetic intensity during the mid-cretaceous from thellier analyses of single plagioclase crystals, *Science,* **291,** 1779–1783.

Tauxe, L., 2006. Long-term trends in palaeointensity: the contribution of DSDP/ODP submarine basaltic glass collections, *Phys. Earth planet Inter.,* **136,** 223–241.

Thellier, E. & Thellier, O., 1959. Sur l'intensité du champ terrestre dans le passé historique et géologique, *Ann. Geophys.,* **15,** 295–378.

Tominaga, M., Sager, W.W. & Channell, J.E.T., 2005. Palaeomagnetism of the igneous section, Hole 1213B, Shatsky Rise, in *Proceedings of the Ocean Drilling Program (ODP)., Sci. Results,* Vol. 198, pp. 1–15, eds Bralower, T.J., Premoli Silva, I. & Malone, M.J., College Station, TX, doi:10.2973/odp.proc.sr.198.113.2005.

Yamamoto, Y., Tsunakawa, H. & Shibuya, H., 2003. Palaeointensity study of the Hawaiian 1960 lava: implications for possible causes of erroneously high intensities, *Geophys. J. Int.,* **153**(1), 263–276.

Zhu, R., Pan, Y., Shaw, J., Li, D. & Li, Q., 2001. Geomagnetic palaeointensity just prior to the Cretaceous normal superchron, *Phys. Earth planet. Inter.,* **128,** 207–222.

Zhu, R., Hoffman, K.A., Pan, Y., Shi, R. & Li, D., 2003. Evidence for weak geomagnetic field intensity prior to the Cretaceous normal superchron, *Phys. Earth planet. Inter.,* **136,** 187–199.

Zhu, R., Lo, C., Shi, R., Shi, G., Pan, Y. & Shao, J., 2004a. Palaeointensities determined from the middle Cretaceous basalt in Liaoning Province, northeastern China, *Phys. Earth planet. Inter.,* **142,** 49–59.

Zhu, R., Lo, C., Shi, R., Pan, Y., Shi, G. & Shao, J., 2004b. Is there a precursor to the Cretaceous normal superchron? New palaeointensity and age determination from Liaoning province, northeastern China, *Phys. Earth planet. Inter.,* **147,** 117–126.

Zhu, R., Pan, Y., He, H., Qin, H. & Ren, S., 2008. Palaeomagnetism and $^{40}Ar/^{39}Ar$ age from a Cretaceous volcanic sequence, Inner Mongolia, China: Implications for the field variation during the Cretaceous normal superchron, *Phys. Earth planet. Inter.,* **169,** 59–75.